Preferred citation: A. Brandberg and A. Kulachenko. The effect of geometry changes on the mechanical stiffness of fiber-fiber bonds. In **Advances in Pulp and Paper Research, Oxford 2017**, *Trans. of the XVIth Fund. Res. Symp. Oxford, 2017*, (W. Batchelor and D. Söderberg, eds), pp 683–719, FRC, Manchester, 2018. DOI: 10.15376/frc.2017.2.683.

THE EFFECT OF GEOMETRY CHANGES ON THE MECHANICAL STIFFNESS OF FIBRE-FIBRE BONDS

August Brandberg[1] *and Artem Kulachenko*[2]

[1] KTH Royal Institute of Technology (augustbr@kth.se)
[2] KTH Royal Institute of Technology (artem@kth.se)

ABSTRACT

In this work, we discuss the effect of geometry on the compliance of the fibre bond regions against normal and tangent loads. Since the fibre bonds play a key role in defining the paper strength, the compliance of the bond regions can affect the amount of elastic energy stored in the bonds and thus change not only the strength but also the stiffness of paper products under certain conditions. Using finite element simulation tools, we overcome the major difficulty of performing controlled mechanical testing of the isolated bond region and reveal the key geometrical factors affecting the compliance of the bond region. Specifically, we show that the compliance of the fibre-fibre bond is strongly governed by its geometric configuration after pressing. Among the strongest factors is the collapse of the lumen and the crossing angle.

Using the range of obtained stiffness values, we demonstrate the effect the bond stiffness has on the stiffness of the network using fibre-level simulation tools. We show how the dependence of tangent bond stiffness on fibre-to-fibre angle further softens the more compliant cross-machine direction.

INTRODUCTION

Having control over the strength and foldability of paper produced from a given paper pulp is valuable in all manufacturing involving paper or its derivatives. Although experiments on the macroscopic scale can reveal the differences in performance between products, they are often unable to explain the cause of the observed differences. In fact, the observed mechanical response is a function of many coupled parameters intrinsic to the material such as fibre morphology, loading history induced by the process, etc. Distinguishing and quantifying the effect of these parameters is difficult as in situ testing of the individual microscopic network constituents is generally hard and sometimes impossible. Similarly, the isolation or decoupling of a single physical phenomenon contributing to the properties of the final product is a challenging task. One of the most important components of the fibre network is the fibre bond, specifically its strength and finite compliance against directional loads. Testing the response of the bond requires the isolation of the bond region and well-controlled constraints. Since precise operations on the bond level are often impossible, the compliance of the bond and its impact on the properties of the paper products remains largely unexplored. Numerical modelling offers a toolbox for distinguishing the impact of individual factors and performing systematic studies.

The effect of the fibre bond has been observed, for instance, in the work of Page, Tydeman, and Hunt [1], Nanko [2] and A Torgnysdotter, A Kulachenko, P Gradin, L Wågberg [3] focusing especially on the bonded area and mean bond size. The mechanical characterization of the individual bonds and in particular, their elastic response is complicated by the necessity of isolating the bonds during testing to ensure that all the elastic energy is stored in the bond region and not outside it. Such tests with a focus on the elasticity of the bond region have not been reported so far. The indirect measurements of the bonds through ZD testing of paper sheets although correlated with the bond properties include the response associated with fibre bending, which cannot be easily excluded.

Page, Tydeman, and Hunt [1] observed that bonded area and changes in the number of bonds with beating could reasonably account for the associated change in the stress/strain curve and strength. At the same time, it was noted, “no similar effect on bonding has been observed with drying tension, which also markedly changes the shape of the stress/strain curve”. Using efficiency factors, Seth and Page [4] demonstrated that the changes made to the bonds do not affect the shape of the stress-strain curve once scaled with an efficiency factor. The efficiency factor proposed was tested by introducing debonding agents and using various levels of wet pressing, which mainly affected the number of the bonds. The efficiency factor proposed fit well with the experimental data in the cases considered. Tracking the change of the efficiency factor can also be used as a state

variable to account for previous straining history of paper and damage introduced during it [5].

The efficiency factor was defined as a property describing stress transfer between the fibres as shown in Equation (1)

$$E_p = \frac{1}{3} E_f \frac{\rho_p}{\rho_f} \left[1 - \frac{\omega}{L\, RBA} \sqrt{\frac{E_f}{2G_f}} \right] \tag{1}$$

where E_f and E_p are the Young's Modulus of individual fibres and paper respectively (N/m^2), ρ is the density (kg/m^3), ω and L is the mean fibre width and length (m), RBA is the relative bonded area (–) and G_f is the shear modulus of the fibres (N/m^2).

Although this equation provides an indication of the factors influencing the load transfer between fibres, the exact mechanics behind the change in efficiency factor have not been studied owing to the experimental difficulties in quantifying the stress-transfer on the bond level. For example, the transverse shear stiffness of the fibres used in Equation (1) cannot be objectively measured or related to the structural properties of the fibre. It, therefore, remains a fitting parameter in the expression for the efficiency factor. In this work, we approach the bond level mechanics and relate the mechanical response of the individual fibre bonds to the net response.

To the extent that numerical modelling has been used to study the mechanical properties of fibre network before, two strategies can be distinguished. The first addresses bond stiffness by excluding the compliance of the bond region entirely. This approach can be justified by assumption for some types of networks and is found in the work of, e.g. [6]. The second uses an already constructed fibre network model to test the effect of varying the stiffness. This modelling strategy can be found in e.g. [7], [8], [9]. Most of the works focus on other aspects of the fibre network and discuss bond region compliance mainly as a numerical factor without assigning it any physical significance. In case of using beam representation for the fibres, however, the bond stiffness represents compliance of the entire bond region since the cross-section of the beam is assumed rigid against local transverse loads.

Since the mechanical properties of fibre networks stem from the microscopic level it has been approached with rapidly developing modelling tools over the past decades. Fibre networks have been modelled using methods ranging from two-dimensional line surfaces (beginning with [10]) to fully resolved three-dimensional structures captured using microtomography (e.g. [11]). The degree of detail in resolving the fibres adds an inevitable penalty in the form of increased computational cost. In practice, this means that if the geometry of fibres is resolved

completely, the size and the density of the considered network is limited to the extent where the effect of the boundary conditions and fibres cut by the domain boundaries cannot be fully eliminated. Thus, the undesirable effects brought by the limited network size prevent addressing realistic problems.

Describing the individual paper fibres as chains of beam elements in the context of the finite element method has been shown to simplify the mathematical model and is a way to attain networks of relevant sizes [12], [13]. Beam theory allows capturing the three-dimensional character of the network as well as fracture and non-linear material behaviour at a reasonable computational cost compared to a full 3-D volumetric approach. However, it adapts certain kinematic assumptions such as the absence of normal strains in the thickness direction and in-plane shear strain. This means the cross-sections of the beam elements is assumed to be rigid against local normal and tangent loads that the bond regions experience during network loading. In the view of these assumptions, many existing analytical and numerical models based on the beam theory do not consider the finite elasticity of the bond. As the fraction of bonded to total fibre length is high, a significant portion of the fibre volume occupied by the bonds may participate in the deformation through local changes of the cross-section. By extension, the amount of elastic energy stored in this volume can also be considerable. Neglecting that the stiffness of the bond regions is finite can be one reason why models based on the assumption of rigid fibre bonds consistently overestimate the elastic properties of fibre networks.

One of the possible ways to integrate the finite elasticity of the bonds within the framework of the beam theory is to introduce some deformable component between the beams at the place of contact. In the framework of the finite element method, this can be either springs [14] or contact elements based on the penalty formulation [15]. The latter has the advantage of not requiring the beam elements to share nodes and offering the possibility to account for the cross-section of the beams in contact. With either approach, the deformable components placed between the beams capture the compliance of the bond region. To be successfully implemented, it requires input in the form of, for example, a traction-separation law. In this work, we offer an approach for estimating the parameters of such a law by considering the isolated fibre bond subjected to different modes of loading. The stiffness under tangential (shearing) load is of particular interest since previous work indicates this is one of the main failure modes of bonds inside a paper sheet in tension [16]. In other load cases, such as sheet compression, the normal stiffness may be the dominant component.

Beyond finding the parameters for such a law, we also show the importance of separate events taking place during the pressing stage. We do this by decomposing the response and systematically studying the effect of adding or removing features from the model. The aim of these experiments is to provide qualitative recommendations for experimentalists when working with, e.g. image analysis

techniques. To achieve these goals, we model the fibre bond region using a full, 3-dimensional representation of the individual fibres.

METHOD

The mechanical strength of bonds is well recognised as being central to predicting failure strength and elongation at failure [17]. Several attempts have been made at quantifying the bond strength experimentally. Magnusson and Fisher investigated the ultimate strength of individual bonds by constructing fibre crosses from isolated fibres [9]. The force-displacement curve until failure was extracted and modelling was used to assist the estimation of the directional strength of the bond from the measured data. In this and other experiments, the bond was not isolated, which is necessary for discriminating the elastic response in the bond region. Apart from the aforementioned difficulties in precise manipulation, the measurements were shown to be sensitive to the adhesive used for constraining the fibres [18], [19]. The adhesive penetrated the fibre and the test setup needed to be constructed from sufficiently long fibres and as a result the elastic energy was predominantly stored in the fibre volume outside the bond region [20]. Some work has also been carried out specifically on the transverse stiffness of individual fibres but the results are mostly reported for the lateral compression [21]. Our work focuses on the transverse tensile and shear stiffness of the compressed fibre-fibre bond – explicitly taking into account the deformation sequence during compression. This stiffness may not be captured using experimental tools due to the difficulty of isolating the individual fibre bond and enforcing the proper boundary constraints. Indirect measures can be obtained using ZD tests [22] and AFM. Although the initial response of the ZD test may correlate with elastic bond properties, it inevitably includes the bending compliance of the fibres, which cannot be easily excluded by the established experimental techniques. The use of AFM is well suited for hardness tests [23] which can potentially be related to elastic properties of the fibre surface. The tests of the transverse properties of the individual fibres, which have been performed in various configurations ([24] and [25]) can also potentially be related to the bond properties in the normal direction, but not readily to the transverse shear bond properties.

Geometry data for modelling the fibres

We consider the fibre bond region in the proximity of a contact between two fibres. The fibre bonds are formed as a result of pressure applied on the fibre network during the paper making process. In our approach, we form a bond numerically starting with a fibre cross.

The fibres have a complex internal structure. An individual fibre may have a length of 2 mm and a width of 20 to 50 μm [26] with various shapes of the cross-sections. Significant effort has been devoted to qualitatively studying the shape of paper fibres as they undergo mechanical treatment, one of the notable examples being Page who attempted to classify the types of bonds formed between fibres into distinct types based on the relative positions of fibres and their original geometry [27]. The focus of the bond characterization was mostly on the bond area, which is related to the bond and network strength but not much to the stiffness. The availability of 3D micro and nano-tomography enables resolving bonds as volumetric entities. Figure 1 shows examples of the fibre cross-sections extracted with microcomputed tomography from a lab sheet made of CTMP fibres.

Figure 2 shows an example of a single bond created from softwood fibres scanned by nano-tomography [28]. Combined with the mechanical testing, these techniques are promising for relating the bond geometrical properties with its mechanical characteristics.

The shape of the cross-section depends partly on the original shape of the fibre and the loads it experiences during all the stages of papermaking. In this work, we assume the initial stress-free configuration of the fibre to be circular. This makes the definition of the MFA straightforward and represents an upper

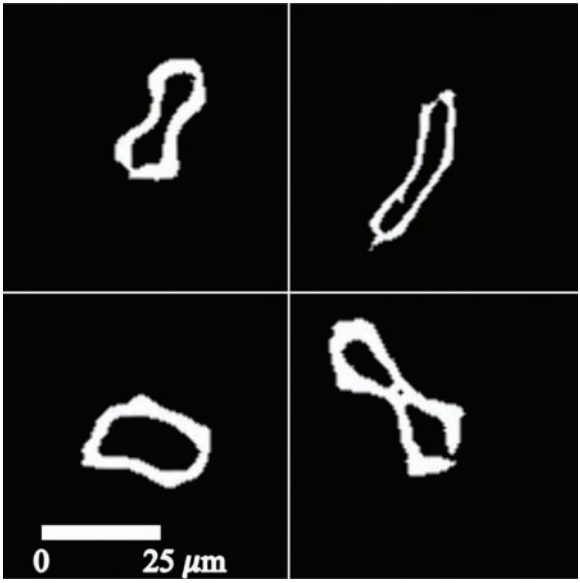

Figure 1. Four fibre cross sections along the unbonded segments of the fibres of a lab sheet made of CTMP pulp captured using μCT with a spatial resolution of 0.5 μm.

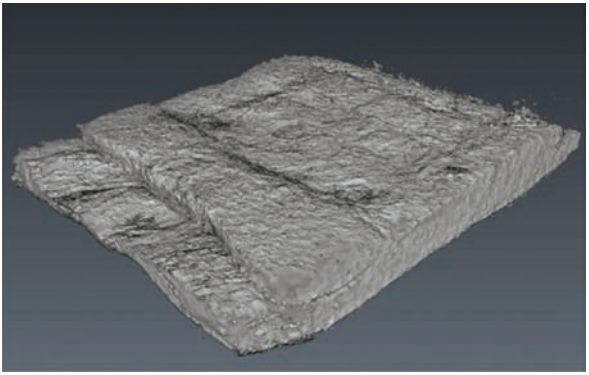

Figure 2. 3D-representation of the bond between two paper fibres captured using nano-tomography. With permission from the authors [16].

bound with respect to the extent of deformation needed to bring the fibre into the final configuration in the bond by applied pressure. We will assess the implication of this assumption through considering the effect of load history induced by compression.

The fibre superstructure is built up of distinct layers referred to as S_1, S_2 and S_3 [29]. The S_2 layer is dominant in terms of volume and gives the fibre the majority of its mechanical properties in particular if the fibre is refined which may damage or detach the outer layers [29]. When representing the fibre in this work, we consider the S_2 layer only. The S_2 layer is characterized by helically wound material where the helical angle is referred to as the Micro Fibril Angle (MFA) with cellulose bundled in fibrils distributed randomly through the thickness. The size of these fibrils is of the order of 5–50 nm [30].

Material data for modelling the fibres

In the elastic regime hemicellulose and lignin are similar as they are both comparatively soft [31]. Lignin exhibits a constitutive response that can be well described by perfect plastic yielding behaviour [32]. The cellulose is considerably stiffer and we assume the yield stress is high. Cellulose and hemicellulose are transversely orthotropic with the stiffest direction aligned with the fibril direction while lignin is isotropic [31]. Several authors have proposed using a law of mixtures formulation to account for what is essentially a helically wound fibre-matrix composite (e.g. [31]). However, to account for dissipative material deformation the rule of mixtures becomes more complex as the effective stiffness of the components change depending on the load history. Our approach is to separate

the material of the S_2 layer into cellulose fibrils represented by orthotropic elastic material and surrounding matrix (lignin and cellulose) which is represented by an orthotropic material with ideal plasticity based on the von Mises yield criterion. The fibres thus consist of two distinct materials. An alternative to this approach is using mixture rules to represent the S_2 layer with a single material [33], which would require homogenization in the linear and nonlinear part of the fibre response.

The material constants of the matrix are determined by applying a mixture rule on the properties of hemicellulose and lignin. We further deviate from the perfectly plastic response by allowing a small measure of hardening of 1% of the elastic modulus as this is strongly beneficial during the numerical solution sequence while altering the stresses and strains of the model only slightly. The fibril content is assumed to be constant along the length of the fibre and is distributed randomly using the Fisher-Yates shuffling algorithm which strictly preserves the designated volume fractions [34]. The material properties used in this study are given in Table 1 where the subscript L refers to the strong direction of the orthotropic material aligned so that the strong direction lies parallel to the axis of the fibril.

Table 1. Material properties of the fibre phases

	Matrix	*Fibril*	
E_L	8.3 [35, 36]	134 [37]	GPa
E_T	4.1 [35, 36]	27.2 [38]	GPa
G	1.3 [35, 36]	4.4 [38]	GPa
ν	0.25	0.1	–
Volume fraction	0.55 [39]	0.45 [39]	
Yield limit σ_y	30 [32]		MPa
Tangent stiffness	40 [32]		MPa

Boundary conditions

Our work aims to capture the response of the fibre bond after pressing and drying. During these stages of papermaking, fibres are subjected to pressure and heat to dewater the fibre mat. A typical peak pressure is about 10–15 MPa on the macroscopic scale [40]. This process is simulated by compressing the fibre-fibre bond from the initially undeformed and stress-free state. While fibres exhibit a strong hygroscopic dependence and are affected by the solid-fluid interaction, describing all the nuances of the process may not be possible (for an extensive review of

hygrodynamic dependence, see for example [29]). The moisture-induced history can significantly affect the final state of the bond. For example, the hygroscopic changes affect the compliance of the fibre-fibre bond prior to the final compressed and relaxed states we examine. Although we do not model the moisture history, we evaluate indirectly the effect it may have by considering different fibre interaction scenarios and the effect of excluding the load history completely.

To capture only the response of the bond, the fibre segments that come into contact during pressing are isolated as in Figure 3. The stiffness contribution of the rest of the fibre is incorporated by preventing out of plane displacement at the open fibre cross-section ends.

The load is applied by rigid plates, which are brought into contact with the fibre-fibre bond and are pressed with a controlled displacement. Parts of the bond that come into contact with the plates are bonded for the remainder of the analysis. The bonding immobilises the wall of the fibre facing the plate, which is consistent with the goal of probing exclusively the mechanical properties of the bond region in the subsequent steps. The complete experimental setup is shown in Figure 3.

The stiffness sought is the stiffness of the fibre-fibre bond after pressing and relaxation. In the final load-step, a displacement is prescribed in either the normal or the tangential direction, as shown in Figure 4.

Finite element solution procedure and result extraction

We use explicit time integration in solving the problem with the finite element method [41]. Unlike implicit integration, which requires inversions of the global

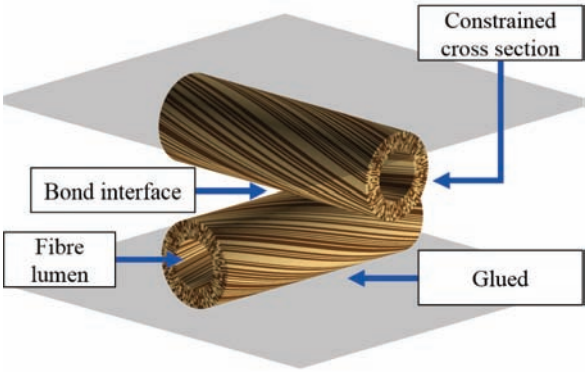

Figure 3. The experimental structure with two fibres at a 90-degree angle to one another and two rigid plates above and below the fibre cross. Lignin indicated in dark and cellulose in light colour.

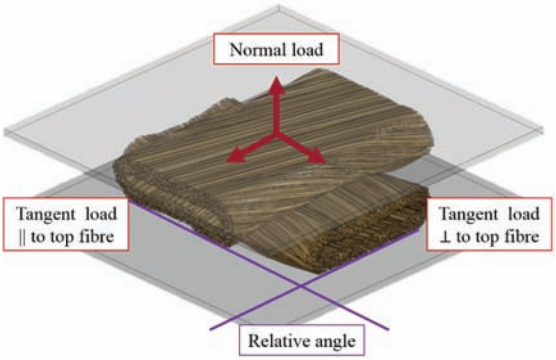

Figure 4. Load application after the compression stage is complete in the normal and tangential direction.

stiffness matrix, the explicit time integration relies on the inversion of the lumped mass matrix, which is trivial and does not suffer from ill-conditioning. However, the explicit integration scheme is only conditionally stable and requires in the considered case a very small time-step due to a fine mesh and the high stiffness to mass ratio of the finite elements. Comparing the performance of the model with implicit and explicit time integration, we selected the latter because both fibres undergo instabilities during the compression and the required load-step becomes too small making the use of the implicit integration very inefficient. We accelerate the solution by increasing the loading rate taking care not to introduce undesirable inertial effects into the model. We ensure that the loading rate is slow enough that the fraction of kinetic to internal energy remains below 2%. The minor high-frequency artefacts present in the response are suppressed through smoothing of the output force using a locally weighted regression algorithm [42].

When undergoing extreme inelastic deformations, the accuracy and numerical stability of finite elements suffer due to poor deformed element shapes. The calculated Jacobian of the elements may turn negative already at moderate deformation, especially when using fully integrated element formulations. While remedies exist, they often amount to accepting lower accuracy (e.g. by using constant stress linear elements) or increased computational time (e.g. adaptive remeshing). To mitigate this problem, we adopt the Element Free Galerkin (EFG) method implemented in LS-Dyna which is more robust for large deformations [43].

A typical force-displacement curve in compression is shown in Figure 5. Two distinct compression stages are visible. In the early stage compression, the fibres are relatively compliant and most of the deformation comes from geometry reconfiguration. The high compression stage is characterised by a stiff material

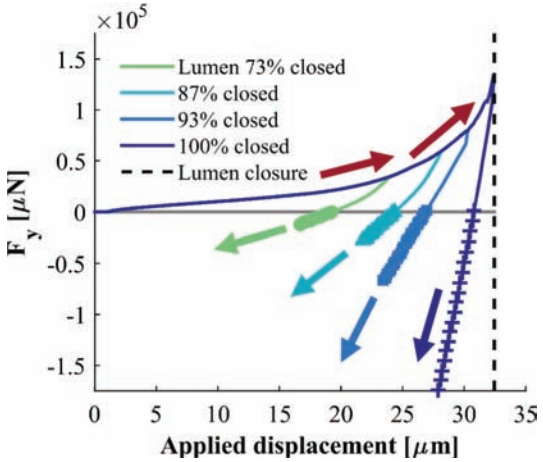

Figure 5. Typical force-displacement curve for a fibre-fibre bond pressed to a successively higher degree. Stiffness is extracted from the linear part of the sections with markers.

response. These features of the response are, in fact, similar to those of individual fibres in lateral compression as shown in [21]. Depending on the ratio of radius to wall thickness the maximum attainable compression varies while the stages of geometry reconfiguration and the features of the bulk response remains the same.

Close to the relaxed state, at which the reaction force on the rigid plate is zero, the effective normal stiffness of the bond region is extracted from the load-displacement response by fitting a first order polynomial to the force-displacement response. The derivative of this polynomial is taken to be the stiffness in either the normal or the tangential direction, depending on which components of the force and displacement vectors that are used.

RESULTS

The developed model can estimate the parameters needed in a traction-separation law between fibres, which can be a direct input to models where fibres are resolved as beam elements. At the same time, it can be used to determine which phenomena on the microscopic length scale dominate in determining the mechanical response of a fibre bond system.

We perform a series of parametric studies where we systematically investigate the influence of the individual factors. In this way, we can quantify the parameters explicitly while at the same time providing guidelines for future work concerning characterization and modification of fibre-fibre bonds.

When the pressing process begins, the fibres are saturated with water, which makes them more compliant. The model does not consider the softening caused by high moisture content meaning the presented forces required to attain lumen closure are overestimated and the stress history prior to relaxation is not captured accurately, with residual stresses being overestimated. In fact, the absolute force needed to attain a specific fibre bond configuration is highly dependent on the load history of the individual fibre inside the network during drying. We assess the impact of stress history by comparing the computed response of the bond with and without residual stresses. At the same time, the presented trends in response to the geometry change will not be significantly affected by not accounting for moisture-dependent properties.

When examining the mesh and fibril size we use a model consisting of two fibres both having the characteristics given in Table 2.

Table 2. Geometry of the reference configuration used to investigate mesh and fibril size dependence

Parameter	*Chosen values*
Inner radius R_{in}	8.00 μm
Wall thickness t	3.50 μm
MFA	16°

The effect of mesh density

The mesh dependence is investigated by refining the mesh for sample geometry. Since the fibril shuffling algorithm is applied to the fibre volume prior to numerical discretization it is possible to keep the same fibril distribution while increasing the number of elements making up each volume. In Figure 6 we show the response of 3 simulations where the cross-sectional area of each fibril volume has been halved and then halved again from an original discretization. As we perform this study only for moderate deformation, we use an implicit solution method to exclude completely any transient effects in the initial response. We apply a displacement of 5.5 μm on a fibre-fibre bond, which has an initial size of 46 μm in the y-direction, corresponding to a transversal compression of approximately 15%.

Beyond the mesh size of approximately 0.4 × 0.4 × 2.5 μm per element the change in response is small and the initial slope of the response is identical, indicating that this mesh is sufficient for capturing the through-thickness gradients. In the remainder of our work, this minimum sufficient mesh density is used to save computational cost.

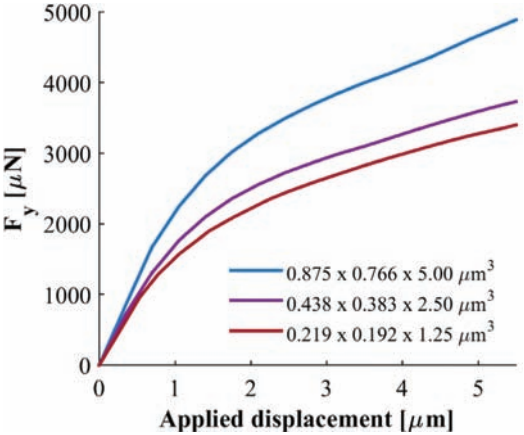

Figure 6. Identical fibril distribution with incrementally doubled mesh density (the dimensions in the legend indicate the mesh size in the radial, hoop and longitudinal direction respectively).

The effect of size of fibril aggregates

Before presenting the result of the parametric study, we investigate the impact of granularity in fibril distribution and find the suitable resolution to represent the matrix and cellulose phase. The individual cellulose fibrils have a cross-sectional dimension of 4×4 nm^2 and are assembled into bundles inside the fibre having a large size of 20×20 nm^2. They may aggregate into large assemblies as a result of chemical and mechanical treatment [44]. In fact, upon assuming a random alignment of the fibril inside the lignin-hemicellulose matrix, some fibrils will end up being closely aligned when the fractions of the matrix and cellulose phases in the fibre are about equal.

The fibril distribution throughout the fibre in the finite element model is not deterministic. Instead, it is assigned randomly based on a shuffling algorithm. Although every fibre realisation is unique, the algorithm preserves the volume fractions of the constituents exactly. With given volume fractions, the response of the considered finite-element model can be affected by the size of the fibrils aggregates and the random distribution of aggregates. In the model, we select the fibril size to ensure the representativeness of the model by examining the initial response of the fibre system during the compression and the resulting normal stiffness. The late stage of the response is affected by the random nature of the fibre structure and nonlinearities of the problem.

The first question we must answer is about how fine the fibril aggregates should be resolved in the modelling. The second question is how much variation that is

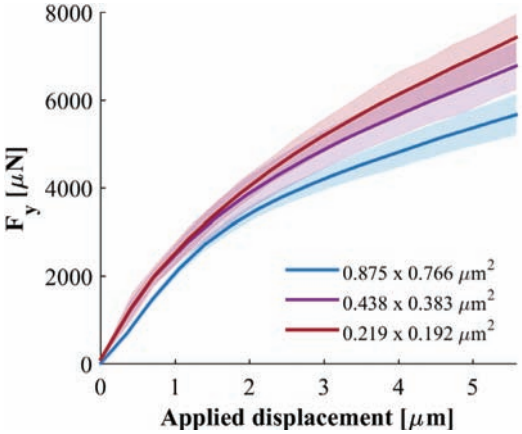

Figure 7. Force-displacement response when refining the fibril aggregates into finer and finer volumes. Shaded area indicates ±1 standard deviation calculated on 5 samples for each run.

induced as the result of random fibril alignment alone. While it is possible to continue splitting volumes into smaller and smaller fibril bundles, the fibril bundles observed in physical samples is computationally infeasible because the small volume size enforces a discretization which is much more refined than is computationally meaningful. Previous work has demonstrated that such a discretization is excessively detailed when capturing the mechanical response of single fibres in axial loading [45]. We perform a similar study in compression with the results shown in Figure 7. As we are interested primarily in the behaviour at moderate compression, we use an implicit solver for this investigation [46]. The same model geometry is used as in the mesh study. The applied 5.5 μm displacement which corresponds to approximately 15% compression.

For the two smaller aggregate sizes the change when splitting each aggregate into 4 new volumes which are independently be assigned either fibril or matrix material is small. At higher deformation, these differences can nonetheless be expected to induce larger changes in the response due to the high non-linearity of the problem.

The random alignment of fibril aggregate

The effect of fibril distribution can be seen in Figure 8, where 5 simulations with identical meshes and fibril fractions are tested using different distributions. Here, we opt to use the explicit method rather than the implicit one in order to be able to apply a higher degree of compression.

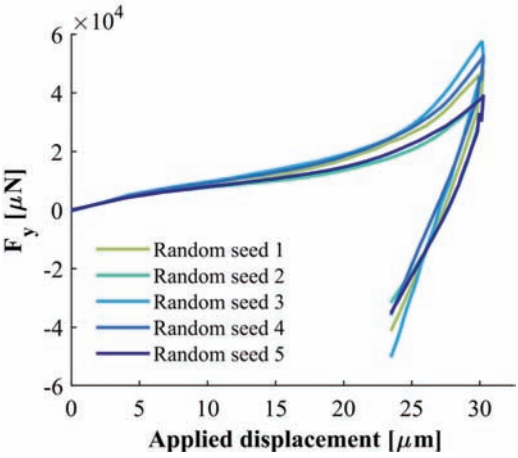

Figure 8. The effect on the mechanical response of varying the distribution of cellulose inside the fibres.

The mean stiffness of the 5 samples at a relaxed state is $1.1 \cdot 10^4$ N/m with the lowest being $0.95 \cdot 10^4$ N/m and the highest $1.4 \cdot 10^4$ N/m which suggests the stiffness varies ±20% due to probabilistic factors alone. The magnitude of distribution dependence is caused by the even fraction of the cellulose to the matrix material. As the fibres compress, dislocations propagate through the more compliant matrix material. In Figure 9 we show how the plastic strain accumulates in narrow bands at the top right and bottom left quadrant of the bottom fibre in the bond with increased applied pressure. With the volume fractions of cellulose and matrix in the fibre being close to even, as in the considered fibre, the formation of the plastic bands will happen with any granularity of the fibrils at some point during compression. The changes in location formation of the band is the main reason behind the discrepancies between the responses for different realizations of the fibre structure observed in Figure 7. Since the variation is unavoidable, the variation in the presented values during the parameter studies can be expected to be around 20% in situations when the change of the parameters alters the alignment of the fibrils.

We perform this simulation with a matrix material softened by a factor 3 as well, to study the influence of the relative stiffness of the constituents and possible softening due to initial presence of moisture. The localization pattern through the thickness of the fibres is not significantly affected for the tested fibres.

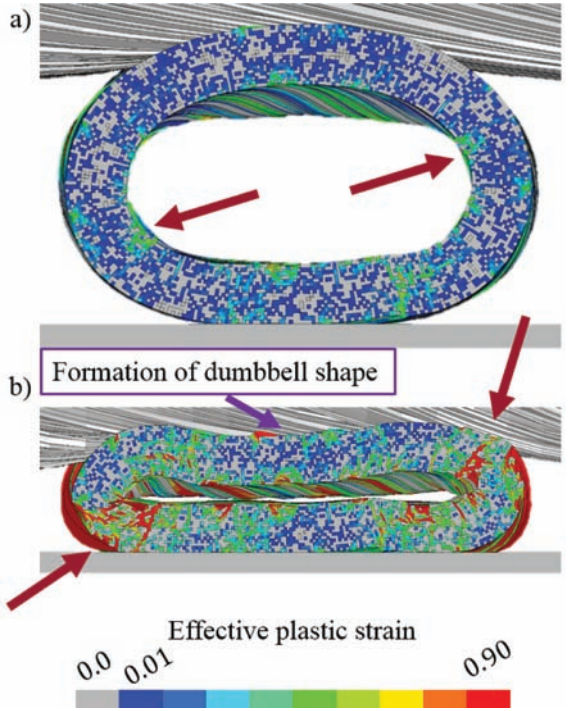

Figure 9. The effective plastic strain in the cross-section of the fibre at (a) moderate compression and (b) high compression. The formation of dislocation bands denoted with arrows can be seen at the bottom left and similarly but more localised in the top right quadrant where lines of highly deformed elements are forming through the thickness of the fibre.

The effect of the fibres original geometry

The response of the bond is influenced by the geometry and the residual stress state. We decompose the change in stiffness that is induced by geometry reconfiguration from the change caused by the stress state and the change caused by the original dimensions of the fibres. We probe the dependence of the fibre bond stiffness to varying radius and the wall thickness within one standard deviation in either direction. In order to extract the data, we use the tomography images of the CTMP fibres and the method described in [33]. Table 2 summarises the input data used.

Horn performed studies on soft- and hardwoods attempting to relate the average micromechanical fibril angle, fibre length, and thickness to the mechanical

Table 3. Chosen geometry parameters for the individual fibres

Parameter	*Chosen values*
Inner radius R_{in}	8.00 ± 3.50 μm
Wall thickness t	3.50 ± 1.25 μm
MFA	(1, 16, 28)°

Table 4. Fibre coarseness calculated for the used geometries

Coarseness $C = A_w \cdot \rho$ [mg/m]			
Inner radius [μm]	*Wall thickness* [μm]		
	2.25	3.5	4.75
4.5		0.206	
8.0	0.194	0.322	0.464
11.5		0.437	

properties of the network. He found that in both cases, the fibril angle and cross-sectional area affected the resulting sheet stiffness [47], [48]. The coarseness of the fibres tested is given in Table 4 where we assume the typical fibre density of 1500 kg/m^3.

A typical reported coarseness value for paper pulp ranges about 0.2, hence the CTMP fibres that are the focus of the present study have a medium to high coarseness.

Luce experimentally studied the collapsibility of model fibres represented as perfectly circular tubes and constructed a shape factor from the outer and inner radius, as stated in Equation (2), where d_o corresponds to the outer and d_i to the inner diameter (m), respectively.

$$SF = \frac{d_o^2 - d_i^2}{d_o^2 + d_i^2} \tag{2}$$

This shape factor was shown to be linearly proportional to the force required to achieve lumen collapse. We perform the same experiment with single fibres using the present model. The results shown in Figure 10 also indicate a linear relation observed in the experiment with model fibres.

We are also in the range of values (110–1030 N/m) for collapse load reported by [21], [50] and [51].

We denote the displacement needed to completely close the lumina with a dashed line. However, the lumen closes partially before this limit is reached due to bulging of the fibre wall as shown in Figure 9b. We indicate this partial lumen closure by filling the symbol and using solid line between the data points. As the

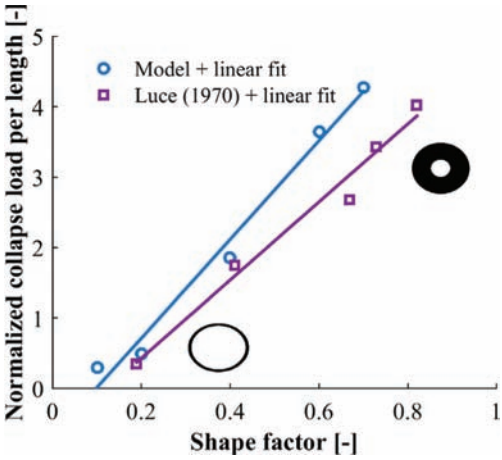

Figure 10. Collapse load versus shape factor for the model (using only a single fibre) and the results of Luce [49].

response is highly non-linear, we have chosen to plot the stiffness on a $\log_{10}$ scale and to facilitate comparison between plots, we keep the axis constant for all cases except the x-axis in the case of changing inner radius.

The effect of radius and wall thickness

Changes in average width and wall thickness of the fibres have a strong effect on the mechanical properties of the sheet. The wall thickness has a direct effect on the density. The response is shown in Figure 11. In Figure 12, we show the stiffness in tangent loading.

At moderate compression, the expected relations hold and the thicker fibre wall exhibits a stiffer behaviour than the specimens with thinner walls. However, as the lumen closes the stiffness increases rapidly and the differences cease to be distinguishable. In other words, the bonds have approximately the same stiffness when the lumina are closed, despite the bulkiest of the geometries having 2.4 times the mass of the thinnest one. The reason behind this is that with the closed lumina, the fibre exhibits the bulk material response, rather than the geometrical stiffness. Another observation is that the tangent stiffness follows the trend of the normal one being approximately equal to half of the normal stiffness at a given degree of compression. The stiffness ranges in the wide range and covers two order of magnitude from the original geometry to the lumen closure.

When varying the radius, the displacement needed to close the lumen varies between the different models and is indicated with a colour-coded dashed line for

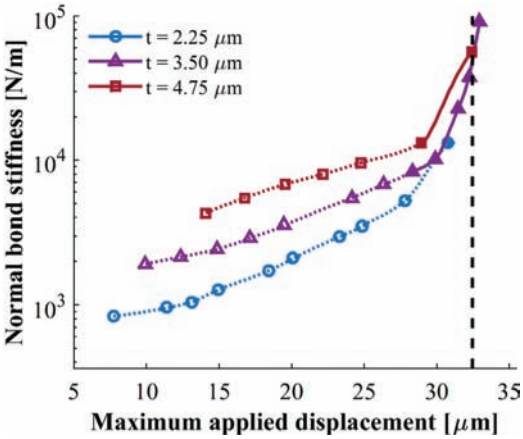

Figure 11. Effect of changing the fibre wall thickness when loaded in the normal direction. The dashed line indicates the displacement required to completely close the lumina. Filled symbol and line indicates partial lumen closure.

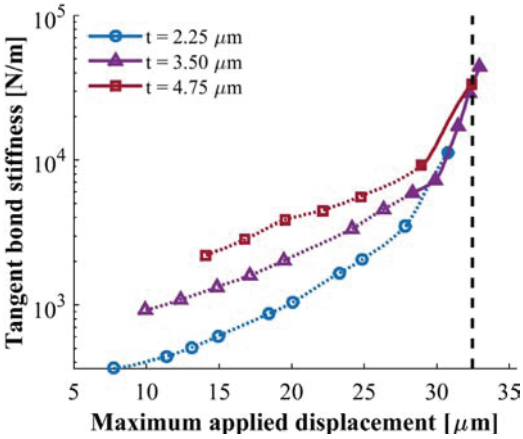

Figure 12. Effect of changing the fibre wall thickness when loaded in the tangent direction. The dashed line indicates the displacement required to completely close the lumina. Filled symbol and line indicates partial lumen closure.

each geometry in Figure 13 and Figure 14. Examining the response for each fibre size the trend remains constant. The radius influences the bond stiffness strongly prior to fibre lumen collapse but the behaviour is dominated by the closure at high compression.

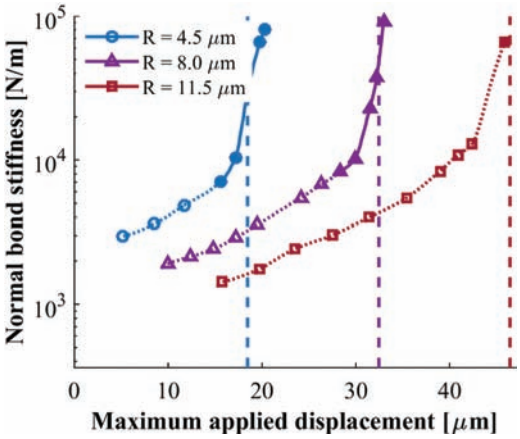

Figure 13. Effect of changing the inner radius when loaded in the normal direction. The dashed line indicates the displacement required to completely close the lumina. Filled symbol and line indicates partial lumen closure.

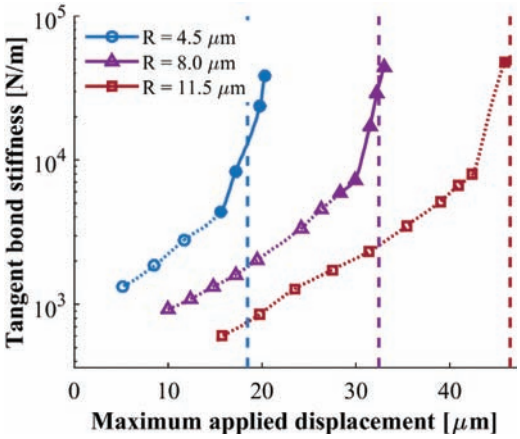

Figure 14. Effect of changing the inner radius when loaded in the tangent direction. The dashed line indicates the displacement required to completely close the lumina. Filled symbol and line indicates partial lumen closure.

An alternative way to consider these results is by presenting the dependence of the bond stiffness on the applied pressure on the bond prior to relaxation. Since the stiffness is governed by the geometry of the fibres, the pressure required to attain certain stiffness will differ with the changes introduced to the fibre, with the diameter being the most influential.

We calculate the pressure using the contact area between the bottom fibre and the plate. The absolute value of the force required to obtain a certain amount of compression is overestimated since we do not consider the softening of the fibres due to hygrodynamic phenomena. Nevertheless, the pressure values can be used to evaluate relative differences. Figure 15 and Figure 16 show the dependence of the bond stiffness on the applied pressure.

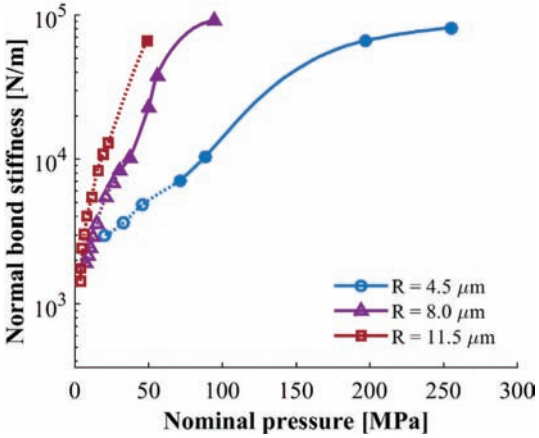

Figure 15. Effect on normal stiffness when changing the inner radius as a function of pressure.

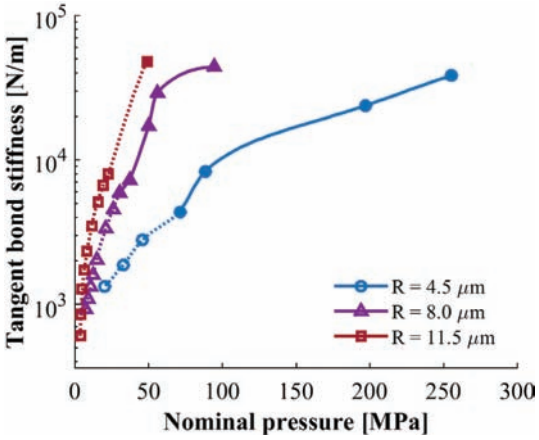

Figure 16. Effect on tangent stiffness when changing the inner radius as a function of pressure.

The amount of pressure required to achieve a higher stiffness increases with decreased diameter of the fibre. This is due to the larger fibres being more compliant which means a smaller force is required to close the lumen. The tangent stiffness follows the same trend. In fact, as we see throughout the parametric studies, the changes in normal stiffness can be used to assess the corresponding changes in the tangent stiffness. At the same time, the normal stiffness is related to the normal response of the fibre, which can be tested using, for example, AFM [52].

Since the stiffness of the bonds is primarily driven by lumen closure, the fibres with initially stiffer geometries will likely form weaker bonds in the final state if a constant amount of force is applied.

The effect of microfibril orientation angle

The microfibril orientation angle (MFA) is recognised as one of the most influential parameters when determining the mechanical properties of individual fibres [53]. For the transverse direction, Bergander and Salmén using small-strain linear analysis found that the MFA of the S_2 layer has a negligible effect on the transverse modulus of the individual fibre [54], [55] and that the matrix properties have a dominating effect. It appears that these conclusions collaborate well with the bond behaviour and agrees with our observations of the relatively small impact of MFA even in the case of large deformation.

The change in bond stiffness as a function of applied displacement during compression is shown in Figure 17 and Figure 18 for different MFAs. The dashed line indicates the point of lumen closure.

It shows that the stiffness is not significantly affected by MFA. There is some difference before the closure because of the reorientation of the material properties. The differences are small because the more compliant matrix material controlling the response has a lower degree of anisotropy compared to fibrils. As mentioned earlier, after the closure of the lumina, the response is mainly driven by the through-thickness properties of the underlying material, the orientation of which are unaffected by MFA.

The stiffening after the lumen closure is increased by an order of magnitude and continues to increase rapidly the fibre is pressed and the self-contact area increases. In the limit, the stiffness of the bond should approach that of a square block of material. Using the outer dimensions of the compressed bond, the estimated upper bond of the stiffness is about $6 \cdot 10^5$ N/m. In other words, the upper limit should be at least a factor 5 higher than the maximum reached in our experiments. Compressing the fibre numerically above certain limit becomes impossible since the volume integration can no longer be performed due to excessive distortion of the matrix material.

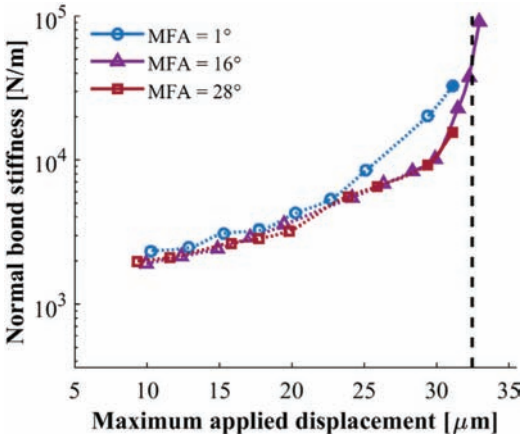

Figure 17. Effect of changing the MFA when loading in the normal direction. The dashed line indicates the displacement required to completely close the lumina. Filled symbol and line indicates partial lumen closure.

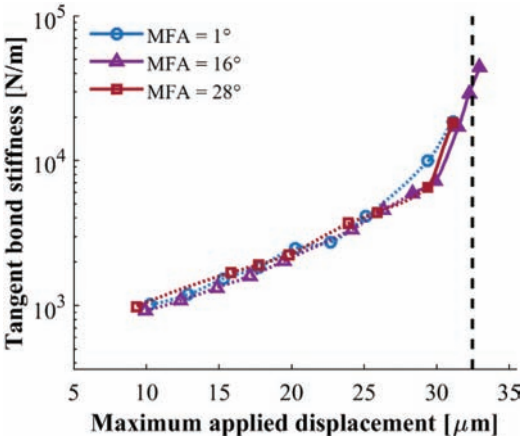

Figure 18. Effect of changing the MFA when loading in the tangent direction. The dashed line indicates the displacement required to completely close the lumina. Filled symbol and line indicates partial lumen closure.

The effect of the residual stress state

During compression, the stresses in the fibre wall cause inelastic deformation of the matrix. Upon removal of the load, the new configuration will contain some

residual elastic strains and, therefore, residual stresses appearing due to inhomogeneous deformation during loading and subsequent unloading. As a result, the fibre material will contain residual strains after relaxation. We evaluate the effect of this stress state by comparing the response of a bond in normal loading after compression with a geometrically identical bond that is subjected to normal loading directly from a stress-free state. After compression, we remove the stress state in the computational environment while preserving the deformed geometry exactly. This effectively converted the deformed stress-free state into the reference configuration. In Figure 19 we show the force-displacement response of a bond tested in the normal direction on the identical fibre with and without the stress-state.

It shows that the stress-free state is softer than the state having residual deformation. By examining the source of discrepancy, we conclude that it is due to the fact the matrix material experiencing elastic unloading in the configuration with the residual stresses, while in the stress-free, it quickly attains the yield stress and therefore shows a more compliant response owing to the small tangent modulus. The difference between the two configurations practically vanishes when the lumina are closed.

In Figure 20 we show the corresponding response but for a bond subjected to tangent loading. Similar to the normal stiffness, the tangent stiffness of the stress-free fibres prior to the lumen closure appeared to be softer than that of the relaxed fibres with residual stresses. The residual stresses stored in the outer layers fibre and the added stress-stiffness contribution do not favour the tangent loading, giving greater tangent resistance before the lumen closure.

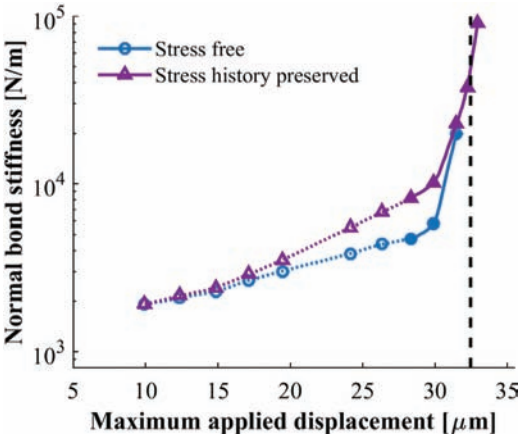

Figure 19. Comparing the response when loading in the normal direction for a stress-free model with one where the complete stress history is preserved.

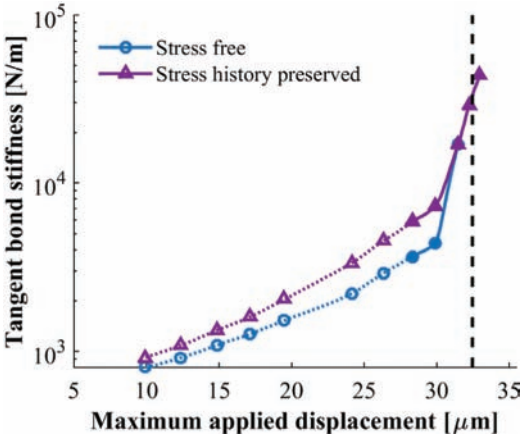

Figure 20. Comparing the response when loading in the tangent direction for a stress-free model with one where the complete stress history is preserved.

The presence of moisture alters the compliance of the structure and not accounting for this change may cause the final stress state in the fibre to be overestimated. Ehrnrooth and Kolseth experimented with measuring the elastic properties of fibres in air and in water. They found that the elastic modulus, measured on the same fibre changed by a factor of 2–3 from wet to dry state [56]. While our model does not directly estimate the size of this inaccuracy, we are able to give both a lower and an upper bound of the effect it may have by considering the extreme case of not having any residual stress after compression. In this case, the stress history is removed from the numerical model before performing the tests.

As seen in Figure 19 and Figure 20, there is a difference in response, especially when the fibres are not completely flattened. However, the size of this difference is not large compared to the effect of fibre geometry, especially considering that the two curves represent the two absolute extreme cases.

All the above studies conclusively demonstrate that in a network containing primarily collapsed fibres, such as a typical paper fibre network, the original geometry of the fibres and the stress state incurred by the deformation influence the stiffness of the bond only to a minor degree.

Effect of differences in compliance between fibres

We further investigate the relation between the fibre-fibre bond stiffness and the geometry of the individual fibres by comparing three bonds subjected to the same load but allowing one fibre lumen to delaminate in one model, both lumina in the

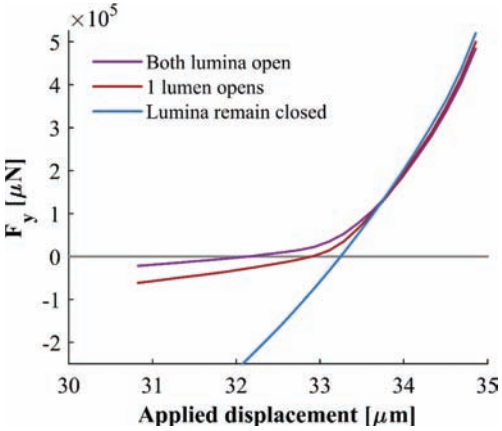

Figure 21. Force-displacement response for fibre bonds where both, one or none of the lumina reopen after compression.

second model and neither lumina in the third model. The results in Figure 21 as expected show that the bond where the lumina remain closed is significantly stronger.

The bond with only one reopening lumen is 3 times stiffer than the completely reopening bond, whereas the bond where both lumina remain closed is more than 11 times stiffer.

The effect of delamination of the lumina on the bond stiffness is smaller when subjected to a tangent load. This is because when loaded in the normal direction the individual fibres may deform in bending which is not possible under tangential load if the fibre is collapsed or almost collapsed.

Very often, the fibre bond is composed of dissimilar fibres. We consider such a case and compare two fibre bonds consisting of identical fibres with a bond composed of one of each. The results are presented in Figure 22 and Figure 23 for normal and tangent load respectively.

Since one fibre is significantly more compliant than the other it will undergo a large degree of compression before stiffening upon lumen closure. This leads to the more compliant fibre lumen closing at a much lower compression than for two identical fibres, where the compression is distributed equally between the fibres. Even before the closure of the lumen, the geometric reconfiguration of the more compliant fibre means it will be significantly stiffer than if two identical compliant fibres were pressed to the same degree.

Seeing the fibres as springs mounted in series is a powerful tool to predict the stiffness of bonds consisting of two types of fibres. In order to apply it in this case of dissimilar fibres, the fibres have to be represented with nonlinear springs in

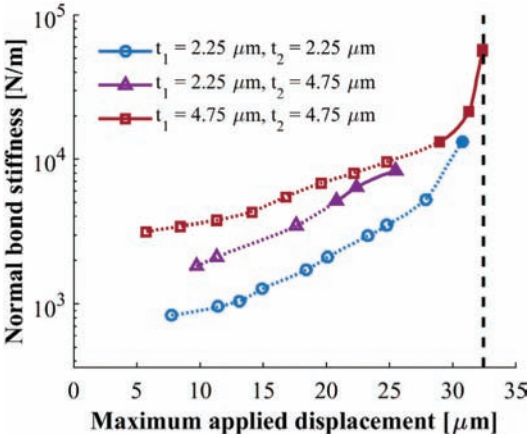

Figure 22. Normal stiffness as a function of applied displacement for thick-walled, thin-walled and mixed-fibre bonds.

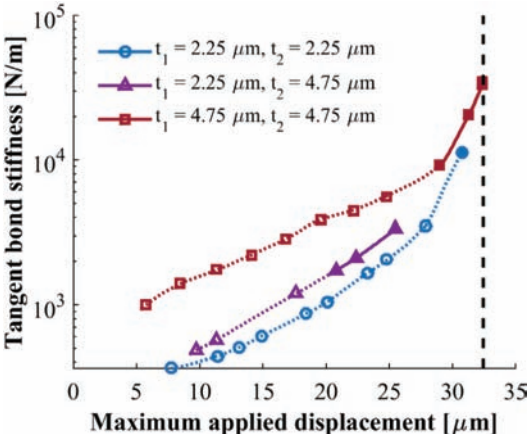

Figure 23. Tangent stiffness as a function of applied displacement for thick-walled, thin-walled and mixed-fibre bonds.

order to identify the deformation state they will end up having in the relaxed configuration as seen from the results above.

The effect of the fibre-to-fibre angle

Not all the fibres are crossing with the 90-degree angle shown in Figure 4. We studied the effect of the fibre-to-fibre angle by varying it in the range of 90 to 10

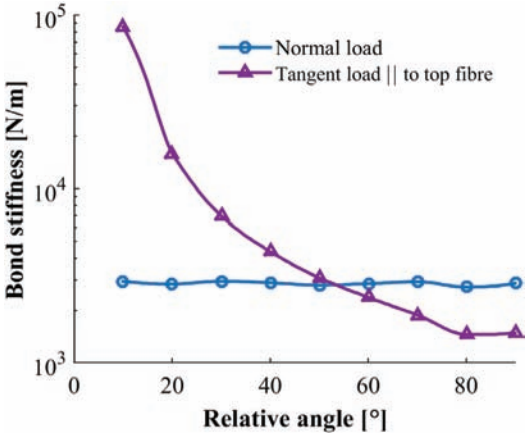

Figure 24. Bond stiffness as a function of the fibre-to-fibre angle for normal and tangent loads.

degrees, probing the stiffness in the direction along the top fibre of the fibres. The results are shown in Figure 24 and are symmetric for the range of angles from 90 to 170 degrees.

The stiffness in the normal direction is independent of the relative angle of the two fibres. As the top fibre is rotated, the only parameter changing during compression is the amount of overlap area, which does not affect the sought stiffness. As the angle is increased, the stiffening increases rapidly as more deformation is transferred along both fibres, that is, in the stiffer direction. In fact, the magnitude of the stiffness becomes significantly greater than in the normal direction. This means, that in the oriented network, the tangent stiffness of the bonds will be greater in the direction aligned with the principle orientation direction of the fibres.

In the view of these results and the effect of the crossing angle, the bond stiffness will have greater influence on the cross-direction (CD) of the network for two reasons: the CD direction is more compliant and there is a greater number of fibres crossing at angles close to 90 degrees [57].

Application at the network level

We artificially create 4 different networks using the fibre deposition methods described in [58]. The goal is to test the effect of the bond stiffness at different densities, grammage and alignment of the fibres. Table 5 summarises the relevant details regarding the generated networks. We use two deposition techniques: In the one referred to as “two-way” deposition, the fibres are deposited from two sides on

the flat surface, which results in a symmetric through-thickness density profile, but most importantly, contained fibres which are relatively straight and are mostly aligned in-plane. In the one-way deposition method, the fibres are deposited on a flat surface from a single direction, which results in two-sidedness with an asymmetric profile. The fibres in this network have to conform to already deposited fibres and therefore, they had greater out-of-plane curvature, which is supposed to make the entire network more compliant due to increased bending of the fibres during tensile loading. The one-sided deposition aims to mimic the hand-sheet forming process.

The differences between the networks are clearly visible in Figure 25 where the cross-sections of the 4 networks are displayed side by side with the order adhering to the one introduced in Table 5.

Table 5. Characteristics of the 4 networks used to evaluate the effect of bond stiffness on the macroscopic scale

Index	*Density* ρ [kg/m^3]	*Grammage* b [g/m^2]	*Deposition method*
1	600	110	Two-way
2	600	55	Two-way
3	300	110	Two-way
4	300	110	One-way

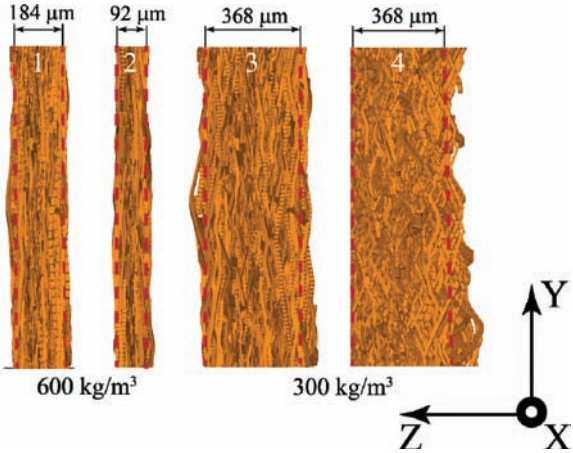

Figure 25. The cross-section of the 4 fibre sheets. From left to right: Dense and heavy, dense and light, sparse and handmade sparse with one-sided deposition of fibres.

The first and the second network have the same density of 600 kg/m^3 but different grammage/thickness. The third and fourth networks have the same density of 300 kg/m^3 but are created with different deposition techniques. Despite using the different deposition technique, the total number of fibre bonds in the third and fourth network is approximately the same.

We perform a tensile test by applying the prescribed displacement, Δu_x, corresponding to a strain level of 0.1% keeping the other edge constrained and the two horizontal edges free as shown in Figure 26.

The size of the network was 8 × 5 mm, which is a representative size for computing the elastic modulus.

The fibre cross-sections are assumed to be solid or hollow rectangular with geometrical properties summarised in Table 3. A constant elastic modulus of E_x = 30 GPa is assigned to all the fibres.

The Timoshenko beam formulation used in the numerical simulation also requires the transverse shear stiffness which is set to $G_{xy} = G_{xz}$ = 3 GPa.

Figure 27 shows how the elastic modulus of the network changes as a function of tangent stiffness presented in the logarithmic scale. In these simulations, we

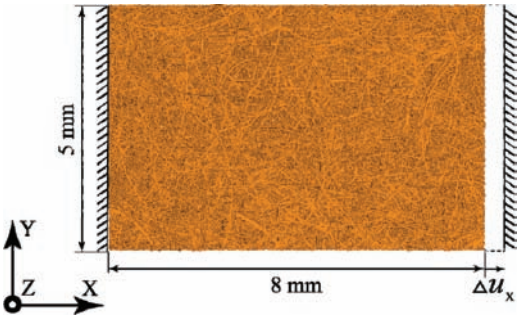

Figure 26. The paper fibre network generated with dimensions and the enforced boundary conditions.

Table 6. Mean geometrical properties of the fibres, length and width of the network and material data used for the fibres

	Mean ± 1 SD
Width	25.537 ± 5.613 μm
Height	14.845 ± 3.428 μm
Width-to-height ratio	1.8469 ± 0.847 [–]
Wall thickness	3.0894 ± 0.753 μm

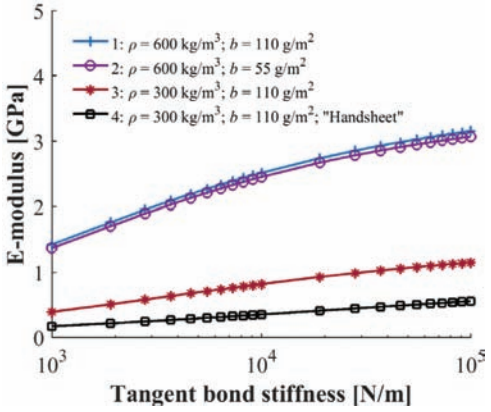

Figure 27. Elastic modulus of the network as a function of the tangent stiffness of the bonds.

assumed that the normal stiffness is 2 times greater than the tangent stiffness and the tangent stiffness is independent of the crossing angle. The influence of the normal stiffness on the tensile characteristics of the network is limited due to shear-type deformation of the bonds dominating [33].

The results show that the elastic modulus is non-linearly affected by the bond stiffness, and the influence is larger in the stiffness range of $10^3 – 10^4$ N/m, which corresponds to the lower range of stiffness recorded for the bonds with the open lumen.

Another important distinction is that the sparse network is more sensitive to changes in the bond stiffness, even though the number of bonds in a sparse network is lower. On the other hand, the sheets with the same density and deposition show indistinguishable response to the changing bond stiffness. At the same time, the one-sided network (denoted "Handsheet" in the plot) shows a lower network stiffness and exhibits a stronger dependence on the stiffness of the bond. This can be seen more clearly in Figure 28, which shows the stiffness reduction factor with respect to the highest value of stiffness captured within the considered range.

The greater sensitivity to the changes in the bonds for sparse or originally more compliant network can be explained by an increased fraction of elastic energy stored in the bonds of such networks. The network with a lower number of bonds and/or more compliant elements in the form of bent or curved fibres will have the elastic energy shifted from stiffer longitudinal deformation of the fibres to more compliant bending and contact deformations. In fact, this transition happens as the stiffness of the network decreases in response to decreased bond stiffness.

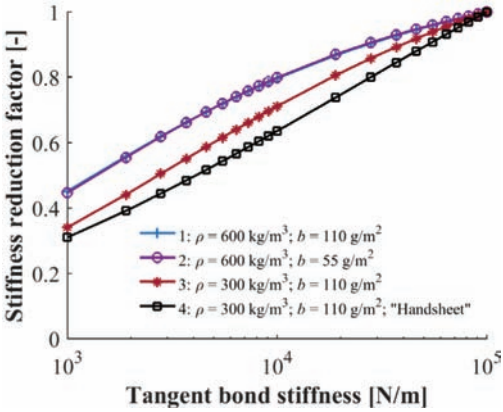

Figure 28. Stiffness reduction factor with respect to the network with the stiffest bonds for each generated network.

Figure 29(a) shows the fraction of elastic energy stored in different forms of deformation at given strain for the dense thick network (network number 1). It shows that decreased bond density leads to an increased fraction of elastic energy stored in the bond regions, which mainly happens at the expense of the energy stored in the longitudinal deformation. Figure 29(b) shows similar information for the sparser network (network number 3). An important distinction explaining a greater effect of the bonds for this network is the greater fraction of the bending energy, which makes the network more compliant in the reference state and therefore the impact of the bond softening is more pronounced.

CONCLUSIONS

Efficiency factors have been a convenient tool to account for the changes brought by bonding to the elastic response of the fibre network. One of the parameters used in deriving the efficiency factors, namely, the transverse shear modulus of the fibres and its relation to the bond geometries has not been previously addressed mainly due to the difficulties of performing direct experiments on the bond level. The role of this property is particularly important for bulky fibres where the geometrical changes of fibres' cross-section can affect the transverse properties of the fibres to a significantly larger extent than observed for elongation properties, which are mainly dependent on the cross-section area rather than its shape.

Using controlled numerical studies performed on the fibre-fibre bond, we find that the directional stiffness of the bond is dominated by its geometrical configuration

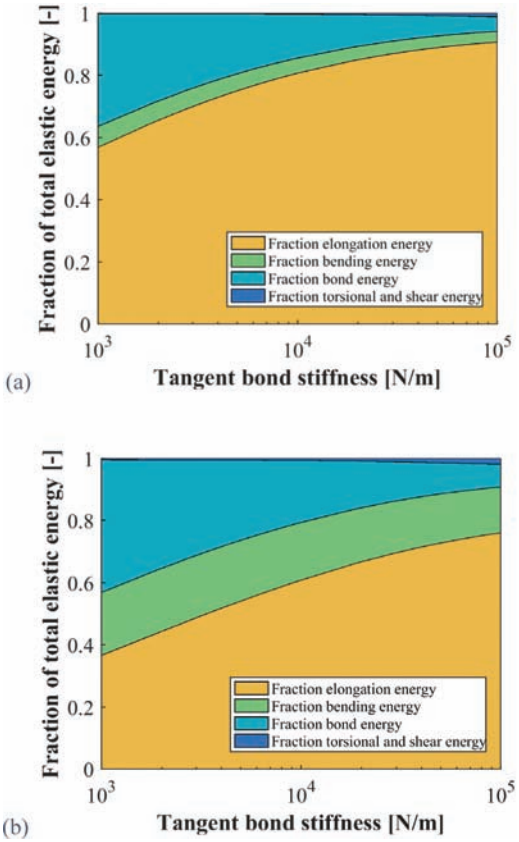

Figure 29. Fraction of the total elastic energy stored in different forms of deformation for (a) a dense network and (b) a sparse network.

as long as the lumina of the fibres in the bond remain open. However, any differences induced by the geometry of the fibres forming the bond have only a secondary impact when the fibres have closed lumina. The closure of the lumen activates the bulk response of the material, which manifests through rapidly increasing stiffness as a function of the degree of compression. The reason behind this is that the closure of the lumen shifts the response of the bond from geometry- to material-driven. When two dissimilar fibres bond, the response will be determined by the more compliant fibre in every configuration since the stiffness of the bond is a nonlinear function of the applied force during bond forming. As the compression progresses, the geometrical configuration causes the fibres to stiffen, which may make an initially more compliant fibre stiffer than the other fibre in the bond.

The crossing angle of the fibres in the bond region does not affect the normal stiffness but has a strong influence on the tangential resistance, which increases rapidly as the angle between the fibres decreases.

Furthermore, while the residual stress state of the fibre-fibre bond may be important in predicting the ultimate strength of the bond, the test of the bond with and without the residual state shows that it has only a moderate effect on the bond stiffness, which means the stiffness can be assessed through its final geometrical configuration.

Finally, the testing of the determined range of the stiffness using network-level simulation tools revealed that the stiffness of the network is almost insensitive to the changes in the bond stiffness corresponding to closed lumina (10^4–10^5 N/m) but shows large sensitivity to the range obtained with open lumina. Furthermore, sparse networks are more sensitive than dense networks owing to a larger part of elastic energy being stored in the more compliant forms of deformation in these networks. This finding is in line with previously reported results based on observations of the effect of the scattering coefficient as a proxy for the degree of bonding, which show that for a given pulp, increased bonding has a strong effect on the elastic modulus in the sparse region and reaches a plateau for the dense region.

Among the most considerable limitations of the present model is not accounting for the transition from a swollen state to a dried state during the compression stage of the bond forming. During drying, the fibre will stiffen and its cross-section will undergo considerable changes due to radial and wall shrinkage. These transformations will inevitably affect the final stress state and configuration of the bond. As we concluded, however, the final configuration has an overall influence on the bond stiffness.

The practical implication of these results is a greater sensitivity to the configuration of the bonds in packaging materials; in particular, the middle ply, which is often composed of bulky fibres and is not exposed to a high degree of compression during manufacture. In addition, in oriented sheets, the CD direction will be more sensitive to the changes in fibre bonds for the reason of being more compliant and having a greater number of fibres crossing at the angles close to 90 degrees.

ACKNOWLEDGEMENT

The financial support from The Swedish Research Council, grant number 2015-05282 is gratefully acknowledged.

REFERENCES

1. Page, D., P. Tydeman, and M. Hunt (1962), A study of fibre-to-fibre bonding by direct observation, in *The Formation and Structure of Paper*, pp. 171–194.

2. Nanko, H. and J. Ohsawa (1989), Mechanisms of fibre bond formation, in *Fundamentals of Papermaking, Transactions of the 9th Fundamental Research Symposium*.
3. Torgnysdotter, A., *et al*. (2007), Fiber/Fiber crosses: Finite element modeling and comparison with experiment, *Journal of Composite Materials*, **41**(13): 1603–1618.
4. Seth, R.P. (1981), DH, The stress-strain curve of paper, in *Trans. VIIth Fund. Res. Symp. Cambridge*, J. Brander (ed.), FRC: Manchester, pp. 421–452.
5. Coffin, D. W. (2012), Use of the efficiency factor to account for previous straining on the tensile behavior of paper, *Nordic Pulp & Paper Research Journal,* **27**(2): 305–312.
6. Bronkhorst, C. A. (2003), Modelling paper as a two-dimensional elastic–plastic stochastic network, *International Journal of Solids and Structures*, **40**(20): 5441–5454.
7. Heyden, S. (2000), *Network Modelling for Evaluation of Mechanical Properties of Cellulose Fibre Fluff*, Vol. 1011. Susanne Heyden, Division of Structural Mechanics, Box 118, 221 00 Lund, Sweden.
8. Wang, C., L. Berhan and A. Sastry (2000), Structure, mechanics and failure of stochastic fibrous networks: Part I—Microscale considerations, *Journal of Engineering Materials and Technology*, **122**(4): 450–459.
9. Magnusson, M. S. (2016), *Investigation of interfibre joint failure and how to tailor their properties for paper strength. Nordic Pulp & Paper Research Journal*, **31**(1): 109–122.
10. Cox, H.L. (1952), The elasticity and strength of paper and other fibrous materials. *British Journal of Applied Physics*, **3**(3): 72.
11. Targhagh, M. (2016), *Simulation of the Mechanical Behaviour of Low Density Paper and an Individual Inter-Fibre Bond*. University of British Columbia.
12. Heyden, S. and P. Gustafsson (2001), Stress–strain performance of paper and fluff by network modelling, in *12th Fundamental Research Symposium, Oxford*, *2001*.
13. Räisänen, V., *et al*. (1996), Elastic-plastic behaviour in fibre networks, *Nordic Pulp and Paper Research Journal* (*Sweden*).
14. Räisänen, V., *et al*. (1997), Does the shear-lag model apply to random fiber networks? *Journal of Materials Research*, **12**(10): 2725–2732.
15. Motamedian, H. R. and A. Kulachenko (2016) *A Robust Algorithm for Normal and Tangential Beam-to-Beam Contact*.
16. Niskanen, K. (1998), *Paper Physics Papermaking Science and Technology*, J. P. Gullichen (ed.), Hannu. Gummerus Printing, Jyväskylä, Finland: Fapet Oy, pp. 162–165.
17. Page, D. (1969), A theory for tensile strength of paper, *Tappi*, **52**(4): 674ff.
18. Fischer, W. J., *et al*. (2014), Imaging of the formerly bonded area of individual fibre to fibre joints with SEM and AFM, *Cellulose*, **21**(1): 251–260.
19. Fischer, W. J., *et al*. (2012), Testing of individual fiber-fiber joints under biaxial load and simultaneous analysis of deformation, *Nordic Pulp & Paper Research Journal*, **27**(2): 237–244.
20. Saketi, P. and P. Kallio (2011), Microrobotic platform for making, manipulating and breaking individual paper fiber bonds, in *2011 IEEE International Symposium on Assembly and Manufacturing (ISAM)*.

21. Hartler, N. and J. Nyrén (1970), Transverse compressibility of pulp fibers 2. Influence of cooking method, yield, beating, and drying, *Tappi*, **53**(5): 820ff.
22. Van Liew, G. P. (1974), The Z-direction deformation of paper, *Tappi*, **57**(11): 121–124.
23. Eder, M., *et al*. (2013), Experimental micromechanical characterisation of wood cell walls, *Wood Science and Technology*, **47**(1): 163–182.
24. Dunford, J. and P. Wild (2002), Cyclic transverse compression of single wood-pulp fibres, *Journal of Pulp and Paper Science*, **28**(4): 136–141.
25. Mikczinski, M., H.X. Nguyen and S. Fatikow (2013), Assessing transverse fibre properties: Compression and artificial hornification by periodic compression, in *15th Fundamental Research Symposium, the Fundamental Pulp and Paper Research Society, Cambridge, 2013*.
26. Mikko, A. and N. Kaarlo (2006), The physics of paper, *Reports on Progress in Physics*, **69**(3): 669.
27. Page, D. and P. Tydeman (1960), Fibre-to-fibre bonds, Part 2: A preliminary study of their properties in paper sheets, *Paper Technology*, **1**(5): 519–530.
28. Retulainen, E. P., Joni; Miettinen, Arttu (2016), X-ray nanotomography of fibre bonds, in *Progress in Paper Physics Seminar, PPPS 2016*, Technische Universität Darmstadt: Darmstadt, Germany, pp. 162–168.
29. Mark, R. E. and J. Borch (2001), *Handbook of Physical Testing of Paper*, *Vol. 1*, CRC Press.
30. Duchesne, I., *et al.* (2001), The influence of hemicellulose on fibril aggregation of kraft pulp fibres as revealed by FE-SEM and CP/MAS 13C-NMR, *Cellulose*, **8**(2): 103–111.
31. Persson, K. (2000), *Micromechanical Modelling of Wood and Fibre Properties*, *Vol. 1013*, Lund University.
32. Rozite, L., *et al*. (2013), Nonlinear behavior of PLA and lignin-based flax composites subjected to tensile loading, *Journal of Thermoplastic Composite Materials*, **26**(4): 476–496.
33. Muzamal, M., E. K. Gamstedt and A. Rasmuson (2014), Modeling wood fiber deformation caused by vapor expansion during steam explosion of wood, *Wood Science and Technology*, **48**(2): 353–372.
34. Knuth, D. E. (1969), *The Art of Computer Programming – Vol. 2: Seminumerical Algorithms*, Reading, MA: Addison-Wesley.
35. Cousins, W. J. (1976), Elastic modulus of lignin as related to moisture content, *Wood Science and Technology*, **10**(1): 9–17.
36. Cousins, W. J. (1978), Young's modulus of hemicellulose as related to moisture content. *Wood Science and Technology*, **12**(3): 161–167.
37. Kroon-Batenburg, L., J. Kroon and M. Northolt (1986), Chain modulus and intramolecular hydrogen bonding in native and regenerated cellulose fibers, *Polymer Communications*, **27**(10): 290–292.
38. Mark, R. E. (1967), Cell wall mechanics of tracheids, *JSTOR*.
39. Norman, B. (1991), *Pappersteknik*, J. A. Bristow (ed.) and p. Tekniska högskolan i Stockholm. Institutionen för, Stockholm: Institutionen för pappersteknik, Tekniska högsk.

40. Holik, H. (2006), *Handbook of Paper and Board*, John Wiley & Sons.
41. LS-DYNA, *Version R9.1.0*. 2017, Livermore Software Technology Corp.: Livermore, CA 94551.
42. MATLAB, *Version 8.5.0*. 2015a, The MathWorks Inc.: Natick, Massachusetts.
43. L.S.T.C. (2017), *43. Element Free Galerkin*, in *LS-DYNA Theory Manual*, pp. 40(1)–40(10).
44. Hult, E.-L., T. Iversen, and J. Sugiyama (2003), Characterization of the supermolecular structure of cellulose in wood pulp fibres, *Cellulose*, **10**(2): 103–110.
45. Borodulina, S., A. Kulachenko, and D. D. Tjahjanto (2015), Constitutive modeling of a paper fiber in cyclic loading applications, *Computational Materials Science*, **110**: 227–240.
46. *ANSYS Academic Research*.
47. Horn, R. A. (1974), *Morphology of Wood Pulp Fiber from Softwoods and Influence on Paper Strength*, DTIC Document.
48. Horn, R. A. (1978), *Morphology of Pulp Fiber from Hardwoods and Influence on Paper Strength*, DTIC Document.
49. Luce, J. E. (1970), *Transverse Collapse of Wood Pulp Fibers: Fiber models*, in *Seminar on Physics and Chemistry of Wood Pulp Fibers 1969*, Appleton, WI: Tappi, pp. 278–281.
50. Hardacker, K. W. (1969), Cross-sectional area measurement of individual wood pulp fibers by lateral compaction, *Tappi*, **52**(9): 1742–1746.
51. Nyren, J. (1971), Transverse compressibility of pulp fibres, *Pulp Pap Mag Can*, **72**(10): 81–83.
52. Rohm, S., *et al*. (2014), Thin cellulose films as a model system for paper fibre bonds, *Cellulose*, **21**(1): 237–249.
53. Page, D. and F. El-Hosseiny (1983), Mechanical properties of single wood pulp fibres. VI. Fibril angle and the shape of the stress-strain curve, *Pulp Pap Mag Can*, **9**(4): TR99.
54. Bergander, A. and L. Salmén (2002), Cell wall properties and their effects on the mechanical properties of fibers, *Journal of Materials Science*, **37**(1): 151–156.
55. Bergander, A. and L. Salmén (2000), Variations in transverse fibre wall properties: relations between elastic properties and structure, in *Holzforschung*, **54**(6): 654.
56. Ehrnrooth, E. M. and P. Kolseth (2007), The tensile testing of single wood pulp fibers in air and in water, *Wood and Fiber Science*, **16**(4): 549–566.
57. Niskanen, K. (2012), *Mechanics of Paper Products*, Berlin and Boston, MA:Walter de Gruyter.
58. Borodulina, S., *et al*. (2016), Extracting fiber and network connectivity data using microtomography images of paper, *Nordic Pulp & Paper Research Journal*, **31**(3): 469–478.

Transcription of Discussion

THE EFFECT OF GEOMETRY CHANGES ON THE MECHANICAL STIFFNESS OF FIBRE-FIBRE BONDS

August Brandberg[1] *and Artem Kulachenko*[2]

[1] KTH Royal Institute of Technology (augustbr@kth.se)
[2] KTH Royal Institute of Technology (artem@kth.se)

Daniele Oliveira de Castro Student at KTH Royal Institute of Technology

Not really a question, but more of an observation, it relates to the shear stiffness relative to the compressive stiffness, that is what you expect for an isotropic material.

Doug Coffin Miami University, Oxford, OH

I have a question for you. If we think about Seth and Page's efficiency factor for paper, it really comes from, maybe, two different parts. In a sparse network, it's about distribution of load and as we get more and more dense it's about the transfer of load and energy. Now, with your models, can you differentiate efficiencies on different levels of network versus fibre? And, if so, does it match up with the experimental results of Seth and Page?

August Brandberg KTH Royal Institute of Technology

Yes.

Tetsu Uesaka Mid-Sweden University

First of all, I agree it's very important to evaluate exactly the bond stiffness on the thick fibres. This is very much a comment. Here you have two stiffnesses for

bonds; tangential and normal. This is OK if we assume that the bond is an interface. On the other hand, if we have a finite thickness, system, one fibre to the other, then you have other modes of stiffness, such as bending and twisting, where on this axis you can bend and twist it. We have quite a complex structure in the bond. Such stiffness are not straightforward to calculate, but you obviously can calculate for such modes too. And for sparse networks such a mode become more important compared to the tangential and normal stiffnesses, because fibres have more freedom to deform.

August Brandberg

It is an interesting observation because you showed in your presentation some of the deformation modes that can occur in the contact and that is absolutely right. I have shown you today normal and tangential deformations and those are perhaps the first ones you would consider. But there are also other things that can happen to the bond, such as relative rotations in between the fibres and you could easily investigate that using this model as well.

Petri Mäkelä BillerudKorsnas AB

Just for clarification. Did you consider straight fibres in your network simulations?

August Brandberg

I would have to refer to my co-author Artem Kulachenko, but in general the fibres are not straight. I realize that it is very difficult for the audience to actually make out individual fibres, but the fibres here are not straight, they are forming some curve because they have a curl.

Petri Mäkelä

A follow-up question. In Figure 29, you presented stored energies. Which energy category is containing the straightening of the fibres?

August Brandberg

We decompose the strain into the various axial and transversal components resolved in the FEM implementation. Fibre straightening would show up as a combination of these deformation modes.

Doug Coffin Miami University, Oxford, OH

Artem could you comment on it?

Artem Kulachenko KTH Royal Institute of Technology

First of all the fibres are not straight. They are curved and they are also not straight in the Z direction as they conform with each other during the forming deposition process, when we made a network. When they straighten, there is a contribution to elongational energy, but most of the energy is in bending. When you deal with this dense network, the fibres are quite immobilized, there is not much bending going on and that is reflected in the energy distribution. As the density decreases, you have more and more fibre bending, both in plane and out of plane during the straining, and it is also seen in an increased proportion of bending energy.